Bulletin of Geophysics and Oceanography Vol. XX, n. X, pp. XXX-XXX; Xxxxx 20xx
DOI 10.4430/bgo00468

Investigation of TEC anomalies possibly caused by the 6 February 2023 Kahramanmaraş (Turkey) earthquakes with space weather conditions

S. Bülbül

Department of Geomatic Engineering, Konya Technical University, Konya, Turkey

(Received: 23 November 2023; accepted: 25 June 2024; published online: 31 October 2024)

ABSTRACT This study investigates the Total Electron Content (TEC) variations associated with major earthquakes in Kahramanmaraş (Turkey) on 6 February 2023, utilising Global Navigation Satellite System (GNSS) measurements and TEC values published by the Jet Propulsion Laboratory. Covering a 37-day period, including 18 pre/post-earthquake days, TEC values, originally from 15 CORS-TR stations in the earthquake region, were analysed in the gridded version. The study assesses pre/post-earthquake anomalies with the purpose of differentiating TEC changes caused by seismic events from those influenced by space weather conditions (SWCs). The examination of SWCs (disturbance storm time, geomagnetic storm index, GSM interplanetary magnetic field, solar wind speed, pressure, electric field, and proton density) reveals a general pre-earthquake quietness. Positive and negative TEC anomalies observed at the station locations during the study period indicate seismic events as potential precursors. Post-earthquake anomalies on 15 and 16 February 2023 are likely linked to SWCs and aftershocks. The study concludes that earthquake-induced TEC variations manifest approximately 16 days before the event, with positive anomalies, transitioning to both positive and negative anomalies approximately eight days before the earthquake. This suggests an eight-day period as a potential earthquake precursor, emphasising the potential for a future development of an early earthquake warning system through the integrated analysis of TEC variations and SWCs.

Key words: GNSS, ionosphere, Kahramanmaraş earthquakes, space weather conditions, TEC.

1. Introduction

The Global Navigation Satellite System (GNSS) was initially a system that allowed point locations to be determined with high precision. While the GNSS is a positioning technique, in recent years it has become a system that provides information about the medium (atmosphere and ionosphere) it passes through by analysing the GNSS signals. GNSS receivers on the Earth continuously collect data from GNSS satellites that endlessly move around the Earth. In this way, data belonging to before, during, and after seismic events can be obtained. With the help of this data, insights into the ionosphere layer through which GNSS signals pass can be obtained (Başçiftçi and Bülbül, 2022, 2023).

Earthquakes, which negatively impact human lives, often result in casualties and property damage. For this reason, scientists from various disciplines have been conducting research to predict the occurrence of earthquakes. In recent decades, numerous scientific studies have

focused on detecting seismic events, such as earthquakes, through the use of GNSS measurements to monitor changes in the ionosphere (İnyurt *et al*., 2020; Bülbül and Bascitfci, 2021). These studies have revealed abnormal alterations in the behaviour of the ionosphere before, during, and after earthquakes, thus, emphasising the importance of investigating the ionosphere for earthquake prediction.

The ionosphere influences the spread of electromagnetic waves and radio frequencies due to free electrons and a significant number of ionised molecules (Liu and Gao, 2004). Changes in the ionosphere depend on factors such as geomagnetic activity, location, quantity of free electrons, and more. Total Electron Content (TEC) is considered as the most crucial parameter of the ionosphere. The TEC is typically measured in TECU (Total Electron Content Unit), where 1 TECU is approximately equivalent to 10^{16} electrons per square metre (el/m^2). The TEC is affected by various atmospheric, geomagnetic, gravitational, solar, and probably seismic changes. At present, many scientific studies rely on TEC values obtained through GNSS measurements (Başçiftçi *et al*., 2017;, 2018; Tang *et al*., 2018; Ulukavak and İnyurt, 2020; Başçiftçi, 2022, 2023).

In recent years, numerous studies have focused on the relationship between GNSS-TEC anomalies and TEC changes induced by earthquakes under different space weather conditions (SWCs). The following citations are examples of some of such studies: Tariq *et al*. (2019) examined the effects of earthquakes with a magnitude of M_w = 7 or greater in Nepal and the Iran-Iraq border between 2015 and 2017. They correlated TEC changes with various space weather indices, such as the disturbance storm time (Dst), geomagnetic storm (Kp), solar radio flux (F10.7), and auroral electrojet (AE) indices. The study suggested a connection between global ionosphere map -TEC and vertical TEC (VTEC) data and ionospheric anomalies, attributing these anomalies to energy release during the earthquake preparation period. Shah *et al*. (2022) conducted research on earthquakes with a magnitude of M_w = 5 or greater occurring between 2000 and 2020. They calculated TEC and VTEC values from GNSS stations within the earthquake impact areas. The study examined the relationship between these anomalies and the Kp and Dst indices, concluding that anomalies occurring a few days before earthquakes are linked to seismic events. Eroglu (2023a) investigated TEC anomalies caused by the M_w = 7.1 Mid-Atlantic Ridge earthquake and the influence of solar activity (F10.7) and magnetic storm indices [Bz (nT), v (km/s), P (nPa), E (mV/m), Kp (nT), and Dst (nT)] within a specific time frame. The study found a connection between anomalies occurring approximately nine days before the earthquake and the day of the earthquake itself. Eroglu (2022) utilised TEC values from the International Reference Ionosphere (IRI) 2012 model (Bilitza *et al.*, 2014) to calculate anomalies occurring under changes in solar wind parameters and proposed a model that includes the use of artificial neural networks for TEC estimation using solar wind parameters and, then, compared this model with the IRI 2012 model. Khan *et al*. (2022) explored the relationship between GPS-TEC data and Swarm satellite TEC anomalies by considering SWCs such as Kp, Dst, and F10.7 indices. The study indicated that TEC anomalies during calm SWCs are associated with a M_w = 6.5 earthquake in Indonesia and occur 5-10 days before the earthquake. Alcay and Gungor (2020) established a connection between TEC anomalies and SWCs, by analysing TEC values from different GNSS stations during quiet and active days. The study concluded that SWCs influence the formation of anomalies. Eroglu *et al*. (2023) investigated TEC changes in the location of the M_w = 6.6 Bodrum earthquake using CODE-TEC maps. By comparing calculated TEC anomalies with SWCs, the study suggested that anomalies occurring 11 days before the earthquake are related to the seismic event, while post-earthquake anomalies are attributed to aftershocks or geomagnetic storms. Using GPS-TEC data, Morales *et al*. (2020) examined ionospheric anomalies related to earthquakes with a magnitude of M_w = 5.1 or greater in Oaxaca, Mexico, between 2008 and

2015. The study considered the Dst index from SWCs and found that 74% of the anomalies occurring before earthquakes are associated with the seismic event. Chukwuma *et al*. (2021) analysed ionospheric anomalies resulting from the M_w = 9.1 Tohoku earthquake of 11 March 2011. They compared these anomalies with the Kp, Dst, and Solar X-Ray Flux indices, suggesting that anomalies occurring 2-6 days before earthquakes may be related to seismic events. In Eroglu (2023b), TEC anomalies caused by the M_w = 6.5 Samar earthquake, Philippines, were compared with various space weather indices. TEC values from the IRI 2016 model were used to calculate anomalies, and the study proposed that anomalies occurring 11 days before the earthquake may be related to the seismic event.

It is crucial to distinguish changes in the ionosphere resulting from earthquakes from other factors that affect GNSS measurements, such as SWCs. One of the earliest studies on TEC changes and ionospheric anomalies was conducted by Leonard and Barnes (1965) by investigating the impact of the 1964 great Alaskan earthquake. Subsequent research aimed to establish the relationship between seismic activity and ionospheric changes. TEC changes and anomaly analysis have generally relied on Global Navigation System (GPS) and ionosonde data (Zhu *et al*., 2014). The limited availability of ionosonde data (approximately 300 stations) hindered the monitoring of seismic changes. However, in recent years, the use of multi-GNSS data and continuous monitoring options have simplified the exploration of seismic events and GNSS-TEC changes.

This study examined the TEC anomalies supposedly related to two significant earthquakes that occurred in Kahramanmaraş in Turkey on Monday, 6 February 2023, with magnitudes of M_w = 7.8 and M_w = 7.5. To carry out the study, TEC values for the days before and after the earthquakes (37 days in total) were obtained from JPL-TEC maps published by the NASA Jet Propulsion Laboratory (JPL), based on the latitude and longitude of 15 continuously operating reference stations (CORS) located in the earthquake region. Since TEC values are determined by evaluating GNSS measurements, the study also considered the disruptive effects of SWCs during the selected time frame. The results of the study clearly indicated that SWCs had no significant impact on the TEC changes believed to be caused by the earthquake. Subsequently, threshold values for TEC changes were calculated to reveal the days with anomalies. As a result of the study, a possible sketch of the earthquake prediction algorithm was proposed based on anomalies and TEC changes.

2. Space weather condition indices

2.1. Geomagnetic storm index (Kp)

The Kp (*Planetarische Kennziffer* in German) index is used to monitor, measure, and indicate the intensity of changes in the Earth's magnetic field. This index represents the average levels of geomagnetic disturbances in the horizontal components of the Earth's magnetic field. It is derived at three-hour intervals by 13 ground-based magnetic observatories (Menvielle and Berthelier, 1991). It varies from zero to nine, where zero indicates minimum geomagnetic activity, and nine corresponds to extreme geomagnetic storms (Lemmerer and Unger, 2019). Each station at Kp observatories is calibrated according to its latitude and provides a K index associated with the geomagnetic activity measured by magnetometers (Başçiftçi, 2023).

To illustrate the intensity of both observed and predicted geomagnetic activity, a five-level system known as the G-scale is defined by the National Oceanic and Atmospheric Administration. The G-scale ranges from one to five, with G0 being the lowest level and G5 the highest.

According to the Kp index between zero and nine, the following levels of geomagnetic activity are defined: Kp = 5 corresponds to minor storms in G1, Kp = 6 corresponds to moderate storms in G2, Kp = 7 indicates strong storms in G3, Kp = 8 corresponds to severe storms in G4, and Kp = 9 corresponds to extreme storms in G5. The Space Weather Prediction Center issues warnings when geomagnetic activity reaches Kp = 4 or higher (https://www.spaceweatherlive.com/en/help/the-kp-index.html).

2.2. Geomagnetic activity index

The Dst index is the most common index for characterising geomagnetic activity, and its unit is nanoTesla (nT). The Dst index is calculated at hourly intervals by averaging the disturbances in the H component of the Earth's magnetic field and monitored by four observatories around the geomagnetic equator (Myagkova *et al*., 2021). To determine whether a storm is occurring, the Dst index is classified in the following levels: -50 nT < Dst < -30 nT is weak storm, -100 nT < Dst < -50 nT is moderate storm, -200 nT < Dst < -100 nT is severe storm, Dst < -200 nT is super storm (http://roma2.rm.ingv.it/en/themes/23/geomagnetic_indices/27/dst_index).

2.3. Magnetic field variation indices

2.3.1. Bx, By, and Bz indices

The interplanetary magnetic field (IMF), part of the Sun's magnetic field carried into space by solar winds, plays a critical role in determining space disturbances around the Earth, including substorms and magnetic storms (Choi and Lee, 2019). The IMF indices include Bx, By, and Bz. Their unit is nanoTesla (nT). During geomagnetic quiet periods, the Bz component points north, while in active periods, it points south (Alcay and Gungor, 2020). The southward orientation of the Bz component is the primary cause of magnetic storms (Adhikari *et al*., 2019). Gonzalez *et al*. (1994) classified the Bz index into three different scales: severe storm (-10 nT), minor storm (-5 nT), and weak storm (-3 nT) (Ulukavak, 2016).

2.4. Proton Density Index

Plasma density of solar wind refers to the protons carried by radiation storms, and these protons, when transmitted by the Earth's magnetic field, collide near the North and South poles. In regions of high latitudes, these protons can cause interruptions in high-frequency signal communication (Ulukavak, 2016). The unit of the proton density index is Np/cm³, indicating the number of protons passing through a unit volume of 1 cm³. Proton density increases during fast solar wind events and decreases during slow solar wind conditions (Schwenn, 2001). If the proton density exceeds the threshold value of 15 Np/cm³ (Ulukavak, 2016), it is considered an active SWC, and data for this index are typically obtained at a one-hour resolution.

3. Material and method

3.1. Obtaining TEC data ionosphere model

To understand the ionosphere, GNSS signals have been used, resulting in a cost effective and fast method for TEC estimation. GNSS signals are affected by many factors until they reach the

receiver from the satellite. The ionospheric effect is described as follows:

$$L_{1,arc} = L_1 - L_2 = I_1 - I_2 + c(\tau_{R1} - \tau_{R2}) + c(\tau_{S1} - \tau_{S2}) + \frac{c}{f_1} N_{1,arc} - \frac{c}{f_2} N_{2,arc} + \varepsilon \quad (1)$$

where $L_{1,arc}$ is the ionosphere dependent variation. L_1 and L_2 are carrier phase observations in distance units; c is speed of light in vacuum; and I_1 and I_2 are ionospheric delays in units of length at f_1 = 1575.42 MHz and f_2 = 1227.60 MHz; τ_R and τ_S are hardware delays of receiver and satellite, respectively; N_1 and N_2 are integer carrier phase uncertainty; ε represents observational noise with multipath (Ciraolo *et al.*, 2007, Ulukavak and Inyurt, 2020).

The ionospheric effect is frequency dependent and this dependence can be explained with:

$$I = \propto \frac{S_{TEC}}{f^2} \quad (2)$$

$$S_{TEC} = L_{1,arc} - B_R - B_S - C_{arc} - \varepsilon_L. \quad (3)$$

Here S_{TEC} is slant TEC, α is a constant value used to convert from TECU to length units, $\frac{c}{\beta(\tau_{R1}-\tau_{R2})}$ and $\frac{c}{\beta(\tau_{S1}-\tau_{S2})}$ hardware delay for receiver and satellites, respectively, for carrier phase observations; $\left(\frac{1}{f_1^2} - \frac{1}{f_2^2}\right)$ ~0.1m/TECU is the constant used in metre to TECU conversion; $C_{arc} = \frac{c}{\beta f_1} N_{1,arc} - \frac{c}{\beta f_2} N_{2,arc}$ is integer phase uncertainty in ionospheric observations; $\varepsilon_L = \frac{\varepsilon}{\beta}$ indicates noise and multipath error (Ciraolo *et al*, 2007; Ulukavak and Inyurt, 2020).

TEC values can be extracted from global, regional and local TEC maps. The Center for Orbit Determination in Europe (CODE), the European Space Agency Operations Centre, and the JPL are some of the institutes/research centres producing TEC maps (Eroglu and Başçiftçi, 2024).

The JPL Ionospheric and Atmospheric Remote Sensing Group uses data from globally distributed GPS stations to determine TEC values. Ionospheric modelling is based on the assumption of a thin ionospheric shell located approximately 350 km above the Earth (Liu *et al*., 2005). VTEC is modelled on a global grid using a bi-cubic spline in a solar-geomagnetic reference plane. JPL-TEC maps, in IONEX format, are produced with 5° longitude and 2.5° latitude grid resolutions.

TEC data, in IONEX format, is organised to enclose the entire world. From this data set, the TEC values at the desired point can be determined. If the locations (latitude and longitude) of a point are known, the TEC value for the point is determined based on the four nearest TEC values, using two-variable interpolation (Schaer *et al*., 1998). Fig. 1 displays the (IONEX TEC) map interpolation framework (bivariate) using the nearest four TEC data. Interpolation of the IONEX TEC data at the location is performed with four points:

$$E_{int}(\lambda_0 + p\Delta\lambda, \beta_0 + q\Delta\beta) = (1-p)(1-q)E_{0.0} + p(1-q)E_{1.0} + q(1-p)E_{0.1} + pqE_{1.1} \quad (4)$$

where p and q take values between zero and one, $\Delta\lambda$ and $\Delta\beta$ represent latitude differences as grid intervals, λ_0 and β_0 denote initial latitude and longitude values, represent known TEC values, indicates the desired TEC value to be determined.

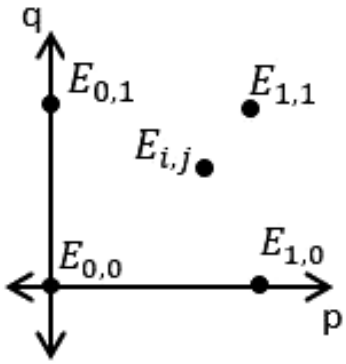

Fig. 1 - The interpolation of $E_{i,j}$ by using the nearest four TEC data.

Global TEC maps provide the TEC values of grid points in 10 TECU units. Therefore, to calculate the TEC value of a desired point from the Global TEC maps, the TEC value calculated by interpolation from the Global TEC maps is multiplied by 0.1. An alternative to the interpolation of TEC values on maps could be to directly use the measurements at each GNSS ground station. In this paper, however, such approach was not followed in order to use already calibrated data from the JPL. After calculating the TEC values, to reveal the existence of any TEC anomaly, first the lower bounder (*LB*) and upper bounder (*UB*) values are calculated with the help of the median (*Med*) value and interquartile range (*IQR*):

$$UB = Med + 1.5\, IQR \tag{5}$$

$$LB = Med - 1.5\, IQR. \tag{6}$$

In Eqs. (5) and (6), setting such bounders ensures that for a Gaussian distribution approximately 95% of samples fall within the range. The presence of an anomaly on any given day is determined if one-third of the TEC values is lower or higher than the bounders. If one-third of the TEC values is lower than the *LB*, that day is considered a day with negative anomaly, and if one-third of the TEC values is greater than the *UB*, that day is considered a day with positive anomaly (Liu *et al*, 2009; Tariq *et al.*, 2019, 2021).

4. Study area

In Turkey on 6 February 2023, two significant earthquakes occurred in the vicinity of Kahramanmaraş. The first earthquake took place in Pazarcık-Kahramanmaraş at coordinates 37.1757° N, 37.085° E at 04:17 local time (LT). Its seismic magnitude was reported by the Ministry of Interior Disaster and Emergency Management Presidency (AFAD) and Kandilli Observatory and Earthquake Research Institute (KRDAE) as being M_w = 7.7, while the United States Geological Survey (USGS) estimated it as M_w = 7.8. The focal depth of this earthquake was reported as 8.6 km by AFAD, 5 km by KRDAE, and 10 km by USGS. The second earthquake occurred in Ekinözü-Kahramanmaraş at coordinates 38.0818° E, 37.1773° N at 13:24 LT. It had a seismic magnitude of M_w = 7.6 according to AFAD, while both KRDAE and USGS reported it as M_w = 7.5. The focal depth for this earthquake was reported as 7 km by AFAD, 5 km by KRDAE, and 10 km by USGS. These earthquakes were strongly felt in various cities, primarily in Kahramanmaraş, as well as Hatay,

Gaziantep, Malatya, Diyarbakır, Kilis, Şanlıurfa, Adıyaman, Osmaniye, Adana, and Elazığ. They also resulted in significant destruction in these affected regions. Kahramanmaraş earthquakes killed at least 50,399 people, injured 115,000 people, and left 1.5 million homeless (https://earthquake.usgs.gov/earthquakes/eventpage/us6000jllz/impact).

In this study, TEC values for 15 CORS-TR stations located in the earthquake region have been calculated using the nearest-neighbour interpolation with the TEC maps published by the JPL (Fig. 2).

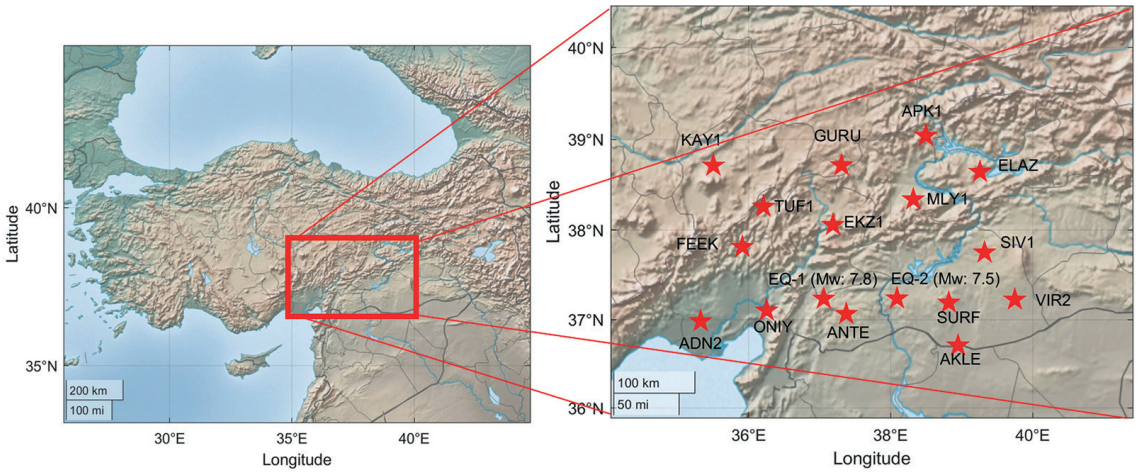

Fig. 2 - The CORS-TR station located at the earthquake area.

5. Results

SWCs with adverse effects on GNSS measurements also have an impact on the estimated TEC values derived from GNSS measurements. Therefore, it is crucial to monitor SWCs in order to discriminate between TEC variations caused by SWCs and those eventually caused by earthquakes. In this regard, SWCs, including Dst, Kp, Bz (GSM), solar wind speed (v), pressure (P), electric field (E), and proton density (N), were analysed for 18 days before and after the earthquakes of 6 February (Figs. 3 to 10).

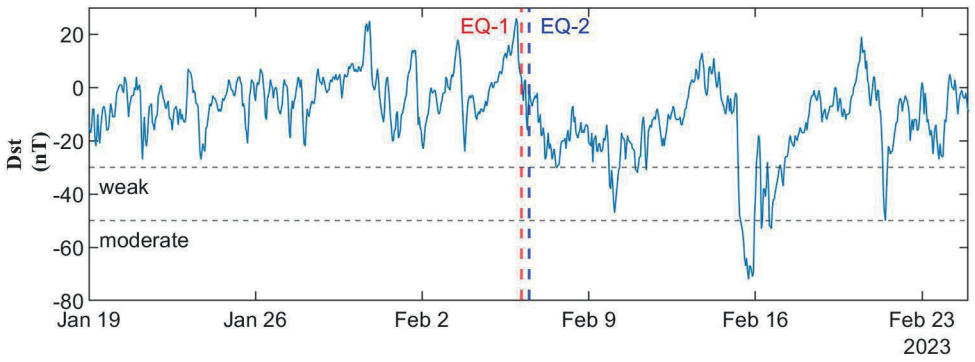

Fig. 3 - Change of Dst index between 19 January 2023 and 24 February 2023.

When examining Fig. 3, it can be observed that the Dst index remained almost quiet until the day of the earthquake, and fluctuating in the range from +26 nT to -27 nT. In this context, it is possible to mention that the Dst index was relatively quiet before the earthquake. However, upon further examination of the same figure, it can be seen that, after the earthquake, between 9 February 2023 (21:00) and 10 February 2023 (06:00), from 10 February 2023 (23:00) to 11 February 2023 (01:00), on 15 February 2023 between 07:00 and 08:00, between 15 February 2023 (23:00) and 16 February 2023 (01:00), on 16 February 2023 between 08:00 and 13:00, between 17:00 and 23:00, on 17 February 2023 from 02:00 to 04:00, on 21 February 2023 between 09:00 and 10:00, and 12:00 weak space weather activities were observed. On 15 February 2023 from 09:00 to 22:00, on 16 February 2023 from 06:00 to 07:00, from 14:00 to 16:00, and on 21 February 2023 at 11:00, moderate space weather activities were observed. Before the earthquake, no strong/moderate geomagnetic activity was recorded, but some very weak geomagnetic activity can be well recognised on 30 January, when Dst increased its value up to +24 nT (the sudden commencement phase of the solar wind impact on the Earth's environment) and, then, drastically dropped to approximately -19 nT and -23 nT on 1 and 2 February, respectively.

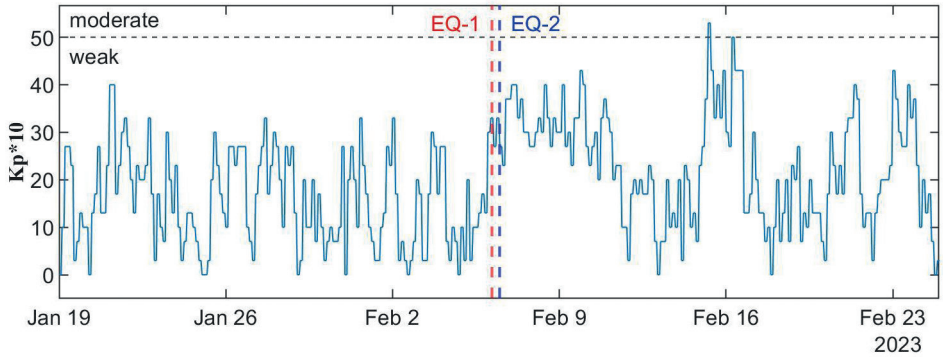

Fig. 4 - The Kp index between 19 January 2023 and 24 February 2023.

When examining Fig. 4, it can be observed that the Kp index remained quiet both before and after the earthquake. However, after the earthquake, weak storm conditions occurred at 06:00 on both 15 February 2023 and 16 February 2023. Before the earthquake, the Kp index ranged from 0 to 4, while after the earthquake, it varied between 0 and 5.33.

In Fig. 5, it can be observed that the Bz index was active on the dates before the earthquake on 19, 22 to 27, and 30 and 31 January 2023, and 1 and 2 February 2023. After the earthquake, the Bz (GSM) index was active on 7, 9, 10, 14 to 16, and 21 February 2023. After the earthquake, the Bz reaches its maximum absolute value at -11.4 nT.

In Fig. 6, it is observed that the solar wind speed reached its maximum speed before the earthquake on 27 January 2023, at 574 km/s. After the earthquake, it reached peak speeds of 611 km/s on 8 February 2023, at 13:00, 528 km/s on 17 February 2023, at 03:00, and the highest point of 661 km/s on 23 February 2023, at 21:00.

In examining Fig. 7, it is observed that the solar wind flow pressure reached its peak value before the earthquake on four occasions (21 January 2023, at 04:00, 26 January 2023, at 11:00, 30 January 2023, at 19:00, and 2 February 2023, at 17:00). After the earthquake, it also reached peak values on 15 February 2023, at 00:00, with 5.41 nPa, and on 15 February 2023, at 04:00, with 5.91 nPa.

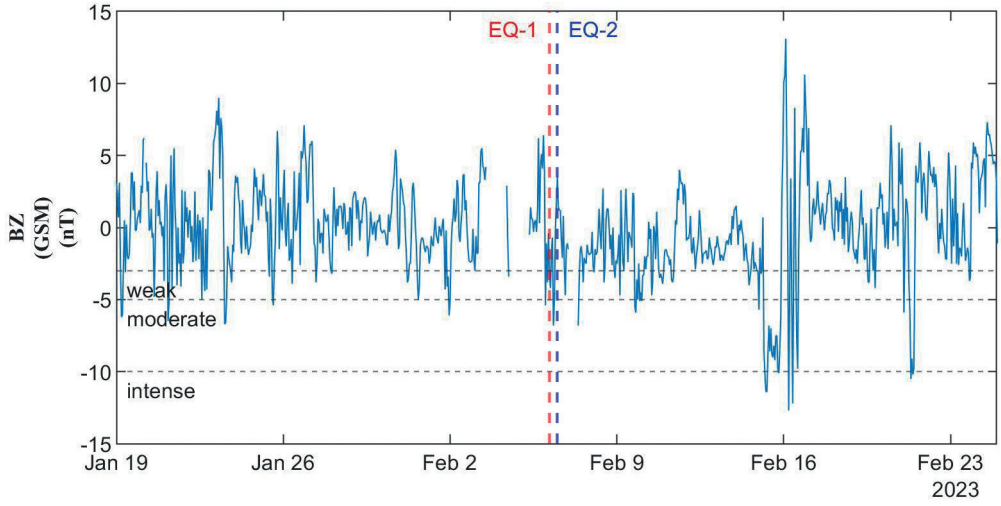

Fig. 5 - The Bz (GSM) index between 19 January 2023 and 24 February 2023.

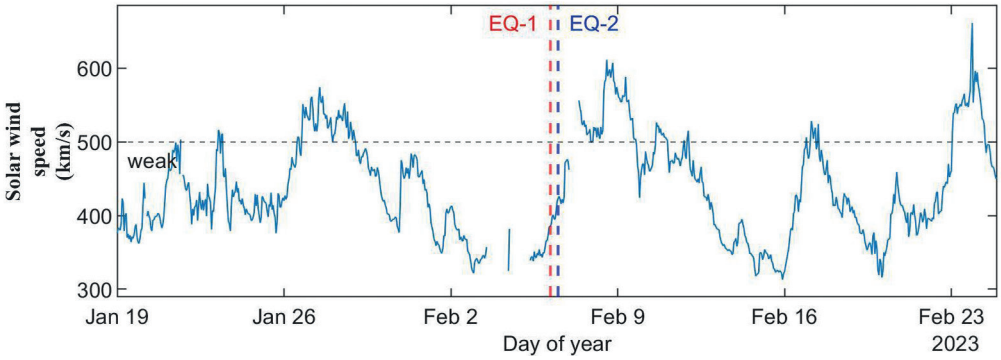

Fig. 6 - The change of solar wind speed between 19 January 2023 and 24 February 2023.

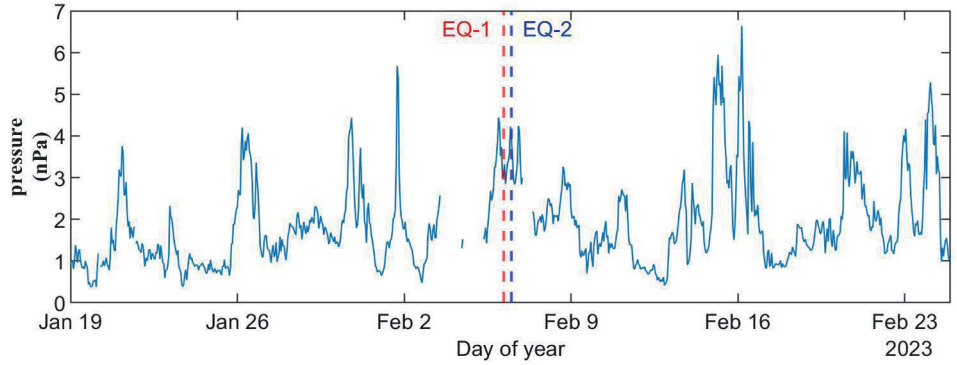

Fig. 7 - The change of pressure from 19 January 2023 to 24 February 2023.

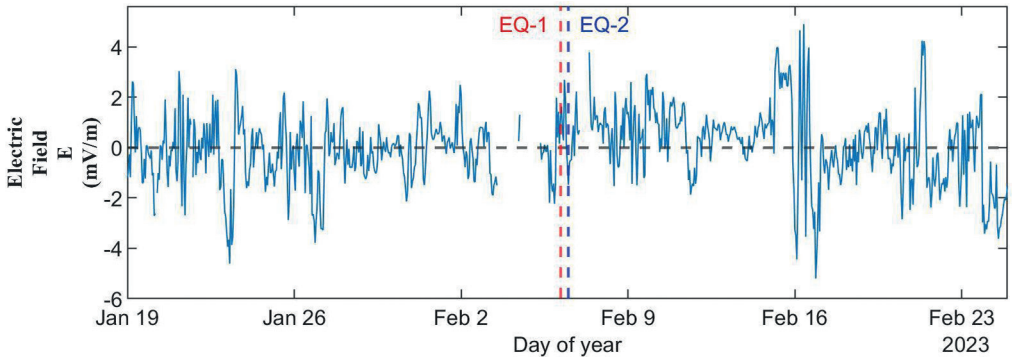

Fig. 8 - The change of electric field from 19 January 2023 to 24 February 2023.

In Fig. 8, it is observed that the electric field had its peak in the negative direction on 23 January 2023, at 07:00, with -4.61 mV/m, and its peak in the positive direction on the same day at 09:00, with 3.11 mV/m before the earthquake. After the earthquake, it first reached the peak in the positive direction, and, then, the peak in the negative direction on 16 February 2023, at 09:00 and 21:00, respectively.

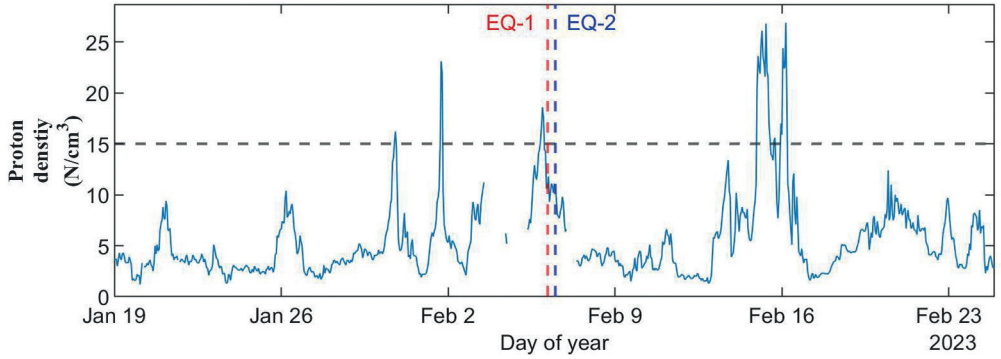

Fig. 9 - The movement of proton density between 19 January 2023 and 24 February 2023.

In Fig. 9, it is observed that the proton density exceeded the threshold value before the earthquake, with values of 15.2 N/cm^3 on 30 January 2023, at 18:00, 23.1 N/cm^3 on 1 February 2023, at 17:00, and 18.6 N/cm^3 on 5 February 2023, from 21:00 to 23:00. Similarly, after the earthquake, the proton density was active and exceeded the threshold value between 14 February 2023, at 23:00 and 16 February 2023, at 05:00.

The duration of activities before and after the earthquake for each day can be observed in Tables 1 and 2.

In examining Table 1, it can be seen that the most active days before the earthquake are from 3 to 5 February 2023. Before the earthquake, the most active activity is related to the Bz (GSM) index and lasts for six hours.

As shown in Table 2, the most active days are from 15 to 16 February 2023. The most active day after these days is on 10 February 2023. The most active index in the table is also the Bz (GSM) index.

Table 1 - SWCs for pre-earthquakes (hour).

SWCs	Days																	
	19 Jan.	20 Jan.	21 Jan.	22 Jan.	23 Jan.	24 Jan.	25 Jan.	26 Jan.	27 Jan.	28 Jan.	29 Jan.	30 Jan.	31 Jan.	01 Feb.	02 Feb.	03 Feb.	04 Feb.	05 Feb.
Bz	3	1	6	4	5		3	1	1	2			5	4	1	1	1	
Np		1	1									2		2		11	22	11
Kp																		
Dst																		
Solar wind speed		1	2		4			8	24	23						11	22	8

Table 2 - SWCs for after-earthquakes (hour).

SWCs	Days																	
	07 Feb.	08 Feb.	09 Feb.	10 Feb.	11 Feb.	12 Feb.	13 Feb.	14 Feb.	15 Feb.	16 Feb.	17 Feb.	18 Feb.	19 Feb.	20 Feb.	21 Feb.	22 Feb.	23 Feb.	24 Feb.
Bz	3	3	7	11	3			5	20	6			4	0	7	0	2	
Np	9							1	16	6								1
Kp									3	3								
Dst	2		3	9	3				17	19	5				5			
Solar wind speed	22	24	19	9	6					1	7						23	11

After analysing the SWCs, the JPL-TEC changes have been investigated.

When analysing Figs. 10 and 11 together, it becomes evident that the first positive anomaly occurred on 19 January 2023, at 12:00 for all stations. The days with positive anomalies are on 21, 22, and 29 January, and 4 and 5 February 2023. Upon comparing the same figures, it can be observed that the first negative anomaly occurred on 26 January 2023, at 22:00 for all

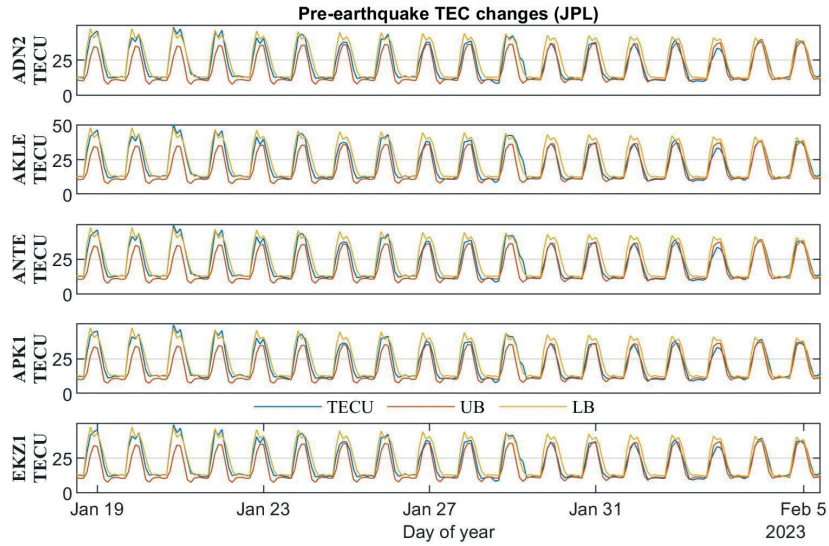

Fig. 10 - The TEC, UB, and LB for ADN2, AKLE, ANTE, APK1, and EKZ1 stations from 19 January to 5 February 2023.

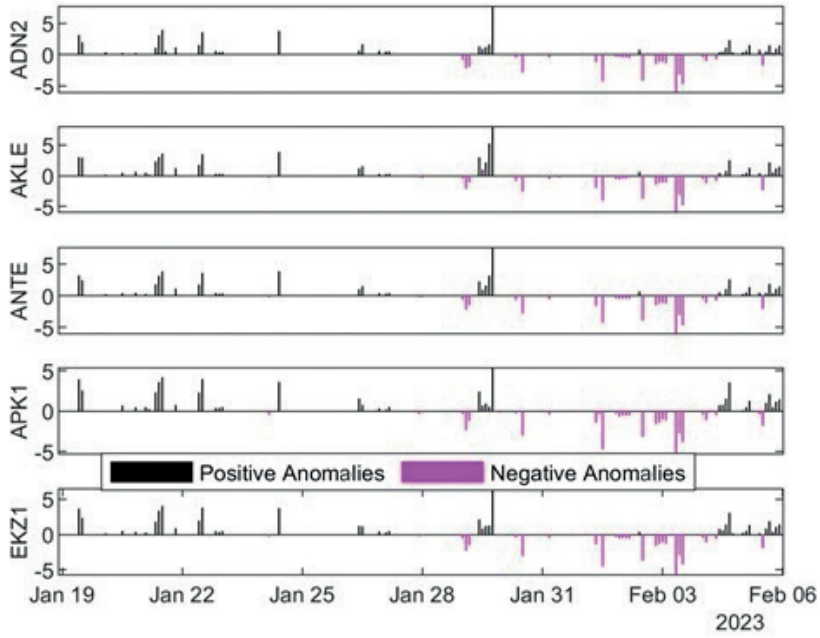

Fig. 11 - The anomaly days for the ADN2, AKLE, ANTE, APK1, and EKZ1 stations (TECU) from 19 January to 5 February 2023.

stations, while the first day with negative anomalies was on 29 January 2023. Furthermore, the days with negative anomalies for ADN2, AKLE, and ANTE are on 29 January 2023, from 1 to 4 February 2023, while for APK1 and EKZ1, it is on 29 January 2023 and from 1 to 3 February 2023.

When analysing Figs. 12 and 13 together, it can be observed that, for the ELAZ, FEEK, GURU, KAY1, and MLY1 stations, the first positive anomaly occurred between 10:00 and 12:00 on 19

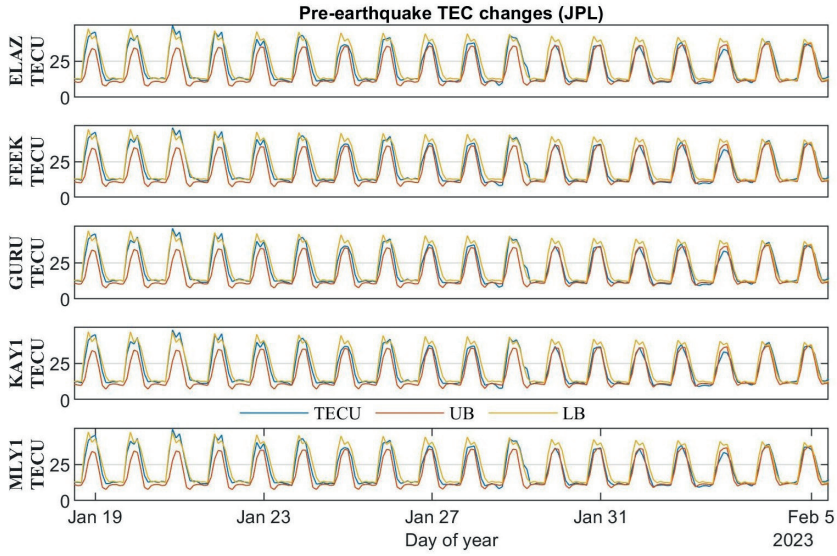

Fig. 12 - TEC, UB, and LB for the ELAZ, FEEK, GURU, KAY1, and MLY1 stations from 19 January to 5 February 2023.

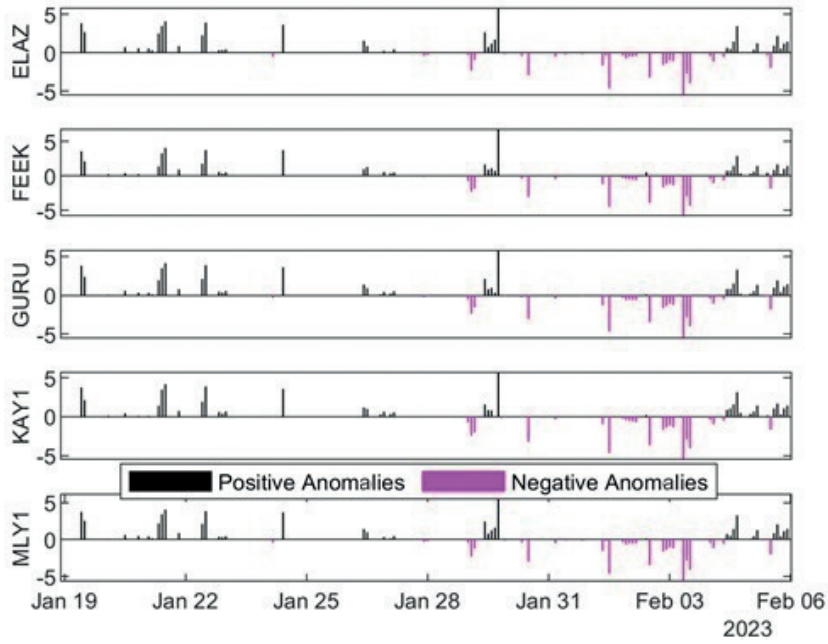

Fig. 13 - The anomaly days for the ELAZ, FEEK, GURU, KAY1, and MLY1 stations (TECU) from 19 January to 5 February 2023.

January 2023. The days with positive anomalies are on 21 and 22 January 2023. For the ELAZ, GURU, and MLY1 stations, the first negative anomaly occurred on 24 January 2023, at 04:00, while 29 January 2023 was the first day with negative anomalies for all stations. Upon further examination of similar figures, it can be seen that the days from 1 to 3 February 2023 have negative anomalies.

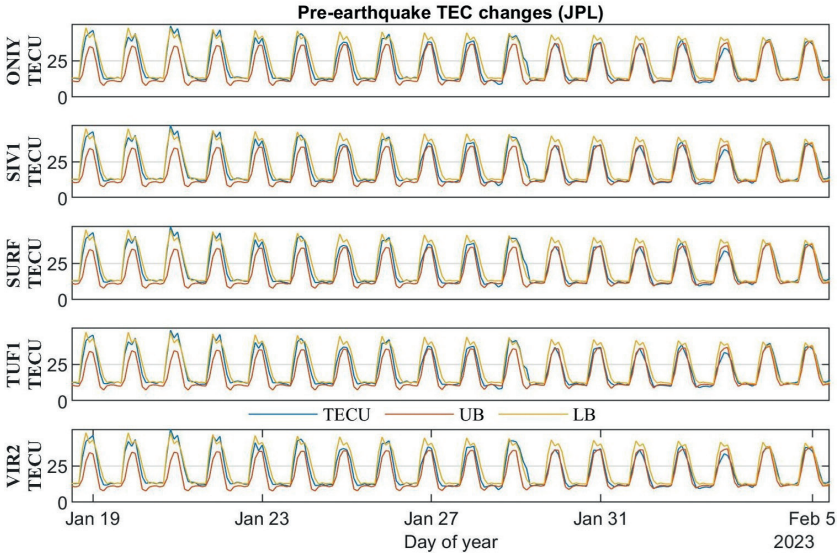

Fig. 14 - TEC, UB, and LB for the ONIY, SIV1, SURF, TUF1, and VIR2 stations from 19 January to 5 February 2023.

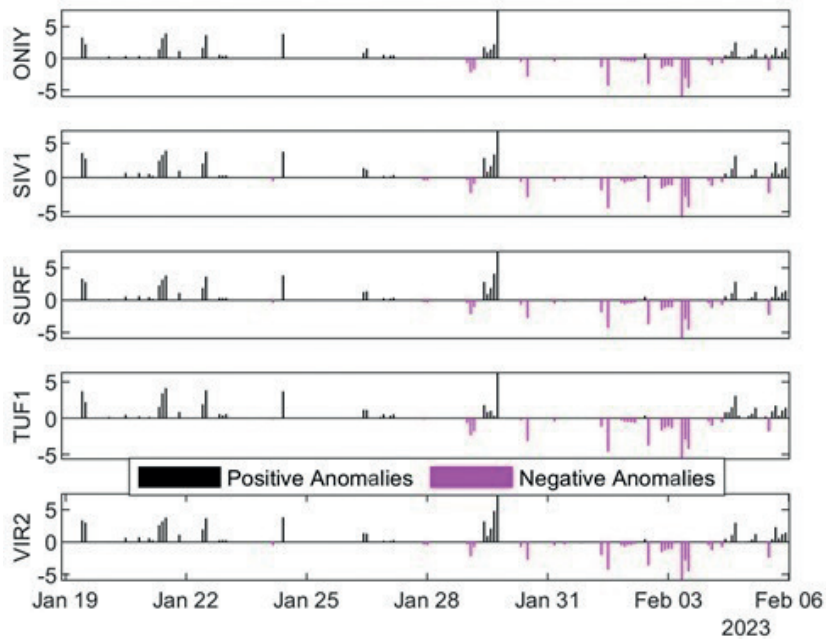

Fig. 15 - The anomaly days for the ONIY, SIV1, SURF, TUF1, and VIR2 stations (TECU) from 19 January to 5 February 2023.

In Figs. 14 and 15, for the ONIY, SIV1, SURF, TUF1, and VIR2 stations, the first positive anomaly occurred between 10:00 and 12:00 on 19 January 2023. The days with positive anomalies are on 21, 22, and 29 January 2023, and 4 and 5 February 2023. The first negative anomaly for the selected stations occurred on 24 January 2023, at 04:00, while 29 January 2023 was the first day with negative anomalies for all stations. Additionally, for the ONIY, SIV1, SURF, and VIR2 stations, the days with negative anomalies are from 1 to 4 February 2023. Only for the TUF1 station, unlike the other days, there were no negative anomalies on 4 February 2023.

Fig. 16 displays the TEC changes at the CORS-TR stations in the earthquake region using interpolation from TEC maps published by the JPL on the earthquake day. When TEC changes are examined, an increase towards noon is observed, followed by a decrease in the evening hours. This indicates that daily TEC variations did not exhibit unusual behaviour on the earthquake day. When the TEC values for the given days are examined, before the earthquake day, TEC values were apparently at a lower level than after the earthquake, and, then, started to increase again.

When examining Figs. 17 and 18, which show the TEC changes and anomalies for stations ADN2, AKLE, ANTE, APK1, and EKZ1 after the earthquake, it can be seen that there were only two days with positive anomalies on 15 and 16 February 2023. In addition, an isolated positive anomaly occurred on 11 February 2023 at 08:00. Negative anomalies occurred on 8 February 2023 at 10:00, 20 February 2023 at 14:00, and on 22 February 2023 from 06:00 to 08:00. From the same figures, it is evident that there were no days with negative anomalies for the ADN2, AKLE, ANTE, APK1, and EKZ1 stations after the earthquake.

When examining Figs. 19 and 20, it is evident that stations ELAZ, FEEK, GURU, KAY1, and MLY1 experienced a positive anomaly on 11 February 2023 at 08:00. After the earthquake, there were only two days with positive anomalies on 15 and 16 February 2023. In the selected stations, there were no days with negative anomalies after the earthquake. However, negative anomalies

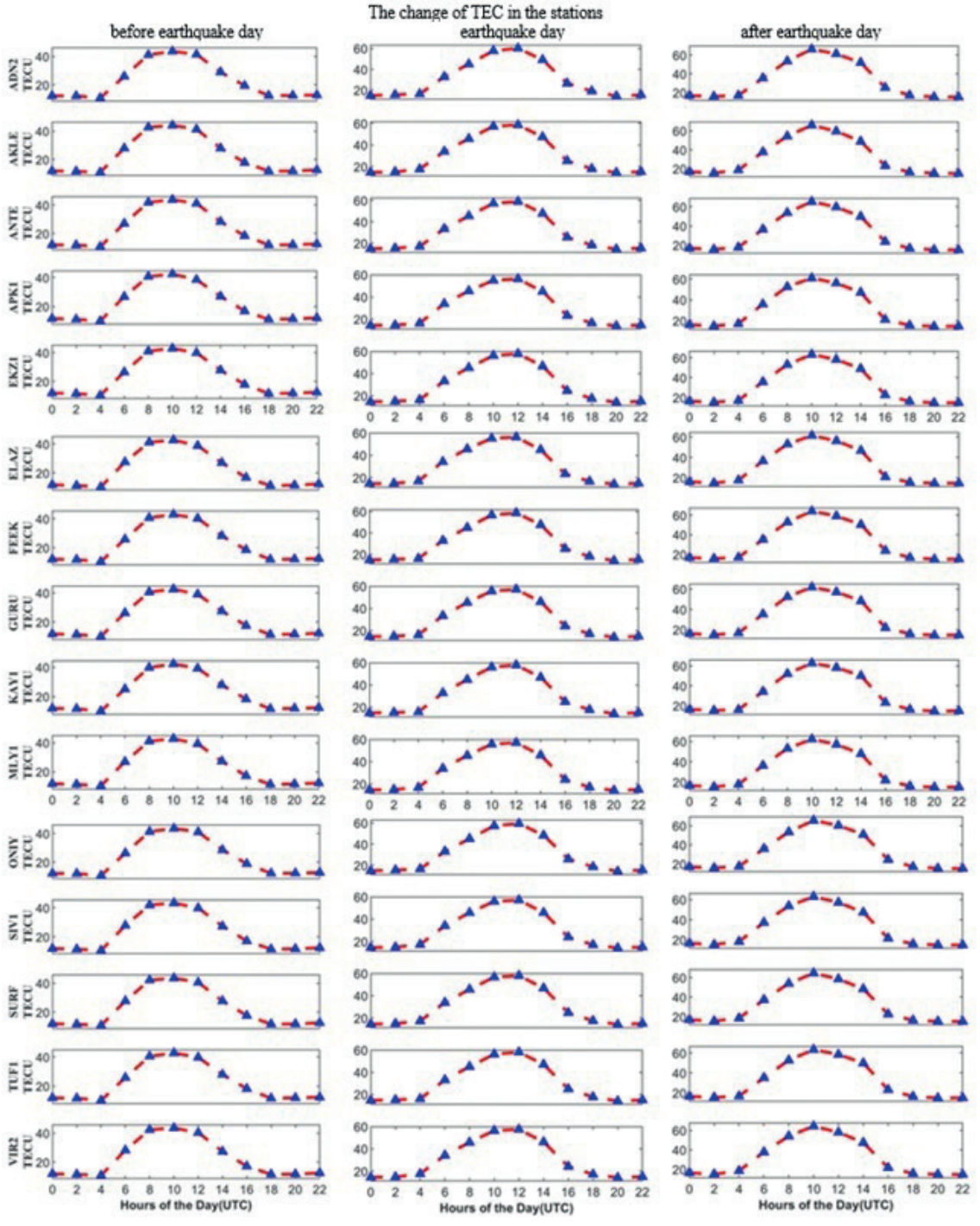

Fig. 16 - The change of TEC in the stations which are located at the earthquake area at before/during/after earthquake.

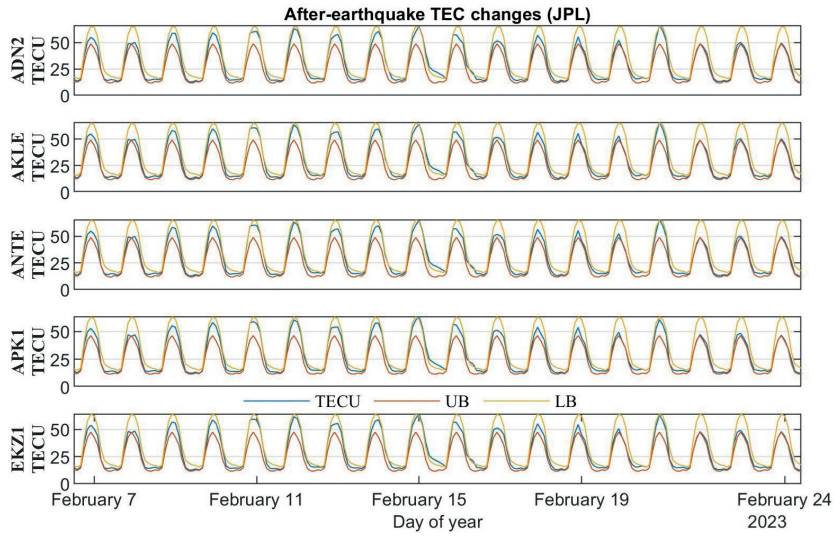

Fig. 17 - TEC, UB, and LB for the ADN2, AKLE, ANTE, APK1, and EKZ1 stations from 7 to 24 February 2023.

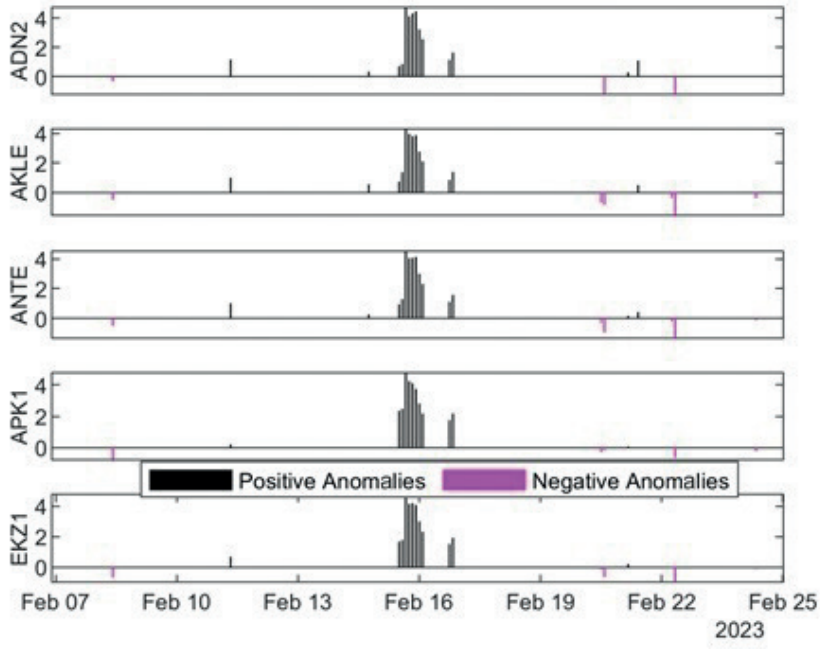

Fig. 18 - The anomaly days for the ADN2, AKLE, ANTE, APK1, and EKZ1 stations (TECU) from 7 to 24 February 2023.

occurred on 8 February 2023 at 10:00, 20 February 2023 at 10:00, and 22 February 2023 from 06:00 to 08:00.

After the earthquake, when examining the TEC variations and anomalies for stations ONIY, SIV1, SURF, TUF1, and VIR2, it is clear that none of the stations experienced days with negative anomalies (Figs. 21 and 22). However, negative anomalies were observed on 8

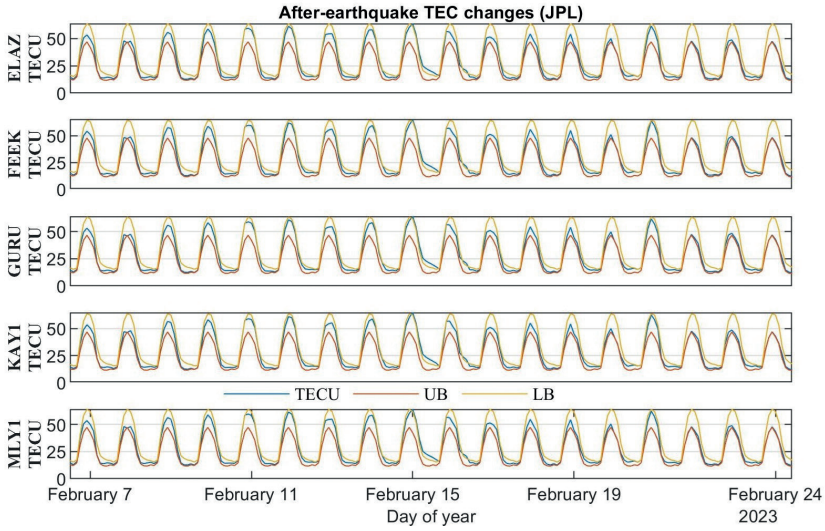

Fig 19 - TEC, UB, and LB for the ELAZ, FEEK, GURU, KAY1, and MLY1 stations from 7 to 24 February 2023.

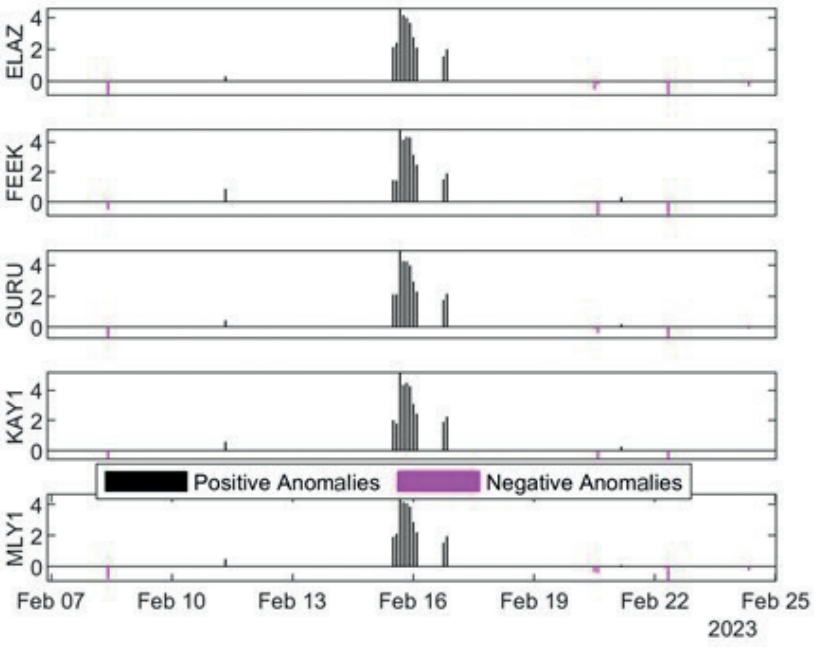

Fig. 20 - The anomaly days for the ELAZ, FEEK, GURU, KAY1, and MLY1 stations (TECU) from 7 to 24 February 2023.

February 2023 at 10:00, 20 February 2023 at 10:00, and 22 February 2023 from 06:00 to 08:00. These stations showed only two days with positive anomalies on 15 and 16 February 2023 (Figs. 21 and 22).

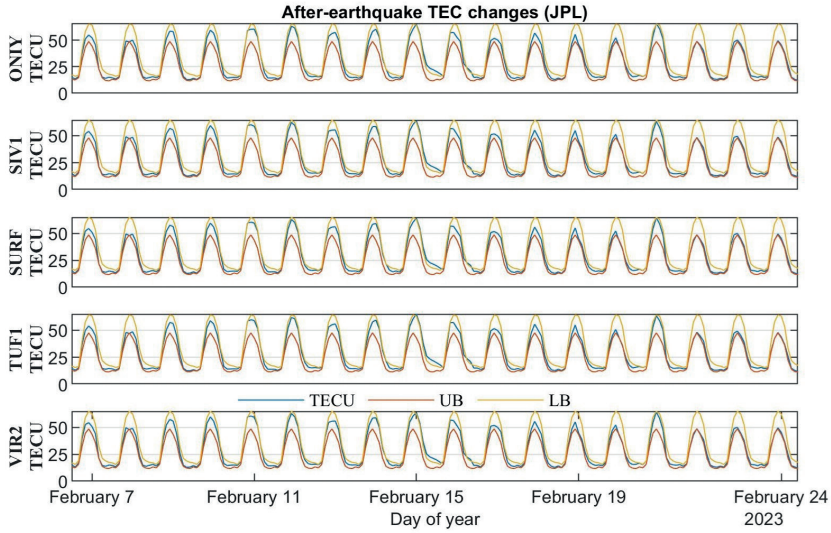

Fig. 21 - TEC, UB, and LB for the ONIY, SIV1, SURF, TUF1, and VIR2 stations from 7 to 24 February 2023.

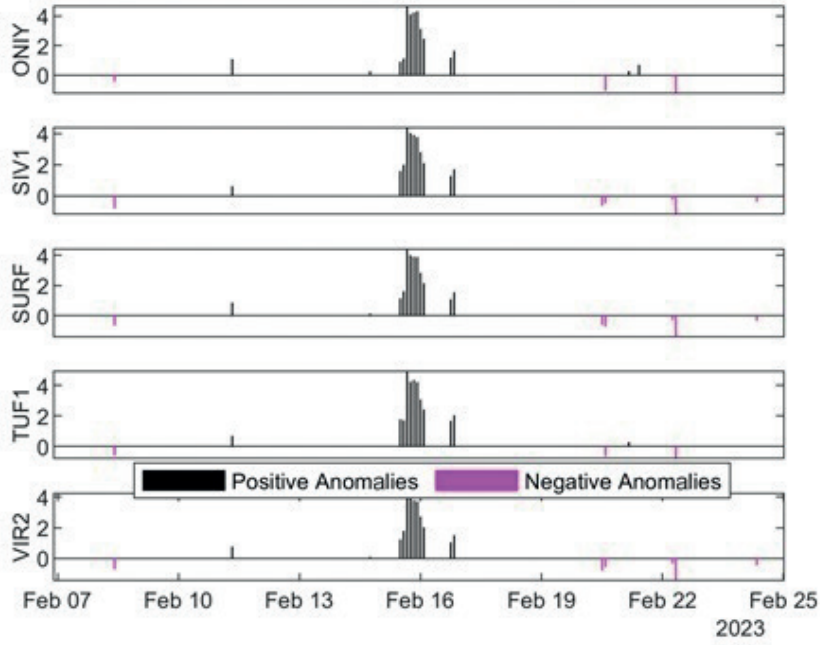

Fig 22 - The anomaly days for the ONIY, SIV1, SURF, TUF1, and VIR2 stations (TECU) from 7 to 24 February 2023.

6. Conclusions

The prediction of earthquakes for disaster prevention is of utmost importance. Thanks to advancing technology, the monitoring of GNSS measurements, and the TEC variations obtained through these measurements, may contribute to the prediction of earthquakes. This claim yields similar to results from our previous studies (Bülbül and Başçiftçi 2021; Başçiftçi and Bülbül, 2022). Determining TEC variations will make it possible to identify anomalies occurring before the earthquake and to determine the days with anomalies. However, one of the most important aspects here is considering SWCs that affect both GNSS measurements and the calculated TEC variations. When identifying TEC anomalies, likely caused by earthquakes, it is necessary to remove anomalies caused by SWCs.

In this study, the TEC variations possibly caused by two major earthquakes (M_w = 7.8 and M_w = 7.5) that occurred in Kahramanmaraş on 6 February 2023, were examined on the basis of TEC values published by the JPL. Future studies can implement an alternative approach directly elaborating the TEC at the single stations to avoid the interpolation in order to improve the precision and accuracy of the obtained results. The study covered a period of 37 days, including 18 days before the earthquake, 18 days after the earthquake, and the earthquake day. During the selected date range, the TEC values of 15 CORS-TR stations located in the earthquake region were determined, and days with positive and negative anomalies occurring on selected days were identified. Additionally, TEC variations were divided into two parts: before and after the earthquake. The study aimed to determine whether the possible TEC change on days with anomalies was due to the earthquake or to the SWCs, and this was carried out using Dst (nT), Kp, Bz (GSM) (nT), solar wind speed (km/s), pressure (nPa), electric field (mV/m), and proton density (Np/cm^3) indices.

During the selected date range, it was generally observed that the Dst (nT), Kp, and electric field (mV/m) remained relatively quiet before the earthquake. In the selected date range, positive anomaly days were observed on 20 January 2023 in all stations, on 26 January 2023 at the APK1, EKZ1, FEEK, GURU, KAY1, and TUF1 stations, and on 29 January 2023 all stations had both positive and negative anomalies. From the Dst trend during these days there had been a very weak impact of solar activity on the Earth's geomagnetic environment. On 31 January 2023, negative anomalies were observed at the AKLE and ANTE stations, and negative anomalies were observed in all stations on from 1 to 3 February 2023. On 4 February 2023, both positive and negative anomalies were observed at the AND2, ANTE, ONIY, SIV1, and VIR2 stations, while some stations had positive anomalies and others had negative anomalies. On 5 February 2023, positive anomalies were observed again in all stations. After the earthquake, almost all indices were active, as clearly shown in Figs. 3 to 10. A similar situation is observed when examining the active hours of SWCs in Tables 1 and 2.

When JPL-TEC variations and days with anomalies are examined together, it is generally observed that TEC variations are likely caused by seismic events, before their occurrence. Still, some of the anomalies could be due to other unknown effects. In addition, some of them, as shown by this study, are due to SWCs. After the earthquake, it can be said that the anomalies that occurred on 15 and 16 February 2023, were influenced by the SWCs (i.e. a weak/moderate storm) that occurred on the same dates and possibly by the aftershocks that occurred after the earthquake.

The most important conclusion that can be drawn from this study is that the impact of a natural disaster, similarly to an earthquake on TEC variations, may begin at least 16 days before the earthquake with a positive anomaly and about eight days before the earthquake causes both

positive and negative anomalies in all stations. In addition, some part of anomalies could be likely related to SWCs. Moreover, the anomalies that started eight days before the earthquake, and continued until the day of the earthquake in almost all stations, can be interpreted as an earthquake precursor. As suggested in this study, the combined analysis of TEC variations and SWCs may contribute to the development of an early earthquake warning system approximately eight days before an earthquake. Our previous studies on the Izmir Seferihisar earthquake and Elazığ/Sivrice earthquakes support this suggestion (Bülbül and Başçiftçi 2021; Başçiftçi and Bülbül, 2022).

REFERENCES

Adhikari B., Kaphle B., Adhikari N., Limbu S., Sunar A., Mishra R.K. and Adhlikari, S.; 2019: *Analysis of cosmic ray, solar wind energies, components of Earth's magnetic field, and ionospheric total electron content during solar superstorm of November 18-22, 2003*. SN Appl. Sci., 1, 453, doi: 10.1007/s42452-019-0474-8.

Alcay S. and Gungor M.; 2020: *Investigation of ionospheric TEC anomalies caused by space weather conditions.* Astrophys. Space Sci., 365, 150, doi: 10.1007/s10509-020-03862-x.

Başçiftçi F.; 2022: *Investigating and comparing the two superstorms in the 23rd solar cycle*. Indian J. Phys. 96, 2707-2716, doi: 10.1007/s12648-022-02396-y.

Başçiftçi F.; 2023: *Using artificial neural networks in the investigation of four moderate geomagnetic storms (mGSs) that occurred in 2015*. Adv. Space Res., 71, 4382-4400, doi: 10.1016/j.asr.2023.01.001.

Başçiftçi F and Bülbül S.; 2022: *Investigation of ionospheric TEC changes potentially related to Seferihisar-Izmir earthquake (30 October 2020, MW 6.6)*. Bull. Geoph. Ocean. 63, 403-426, doi: 10.4430/bgo00394.

Başçiftçi F. and Bülbül S.; 2023: *Statistical analysis of the regional and global ionosphere model on intense geomagnetic storm*. Indian J. Phys., 97, 3395-3409, doi: 10.1007/s12648-023-02700-4.

Başçiftçi F., İnal C., Yıldırım Ö. and Bülbül S.; 2017: *Determining regional ionospheric model and comparing with global models.* Geodetski Vestnik, 61 (3), 427-440, doi: 10.15292/geodetski-vestnik.2017.03.427-440.

Başçiftçi F., İnal C., Yıldırım Ö. and Bülbül S.; 2018: *Comparison of regional and global TEC values: Turkey model*. Int. J. Eng. Geosci., 3, 61-72, doi: 10.26833/ijeg.382604.

Bilitza D., Altadill D., Zhang Y., Mertens C., Truhlik V., Richards P., McKinnell L-A. and Reinisch B.; 2014: *The International Reference Ionosphere 2012 - a model of international collaboration*. J. Space Weather Space Clim., 4, 1-12, doi: 10.1051/swsc/2014004.

Bülbül S. and Başçiftçi F.; 2021: *TEC anomalies observed before and after Sivrice-Elaziğ earthquake (24 January 2020, Mw: 6.8)*. Arabian J. Geosci., 14, 1077, doi: 10.1007/s12517-021-07426-3.

Choi K.E. and Lee D.Y.; 2019: *Origin of solar rotational periodicity and harmonics identified in the interplanetary magnetic field (B{z}) component near the Earth during solar cycles 23 and 24*. Sol. Phys., 294, 44, doi: 0.1007/s11207-019-1433-7.

Chukwuma V.U., Adekoya B.J., Thomas J.E., Emah J.B. and Oloruntola R.F.; 2021: *On the significance of requisite criteria in detecting pre-earthquake ionospheric precursors: a case study of the Tohoku earthquake of March 11, 2011*. Acta Geophys., 69, 1545-1566, doi: 10.1007/s11600-021-00627-0.

Ciraolo L., Azpilicueta F., Brunini C., Meza A. and Radicella S.M.; 2007: *Calibration errors on experimental slant total electron content (TEC) determined with GPS*. J. Geod., 81, 111-120, doi: 10.1007/s00190-006-0093-1.

Eroglu E.; 2022: *Discussing total electron content over the solar wind parameters*, Mat. Prob. Eng., 2022, 1-14, doi: 10.1155/2022/9592008. Eroglu E. and Başçiftçi F.; 2024: *Mathematical modeling of the Southeastern Turkey earthquake (Pazarcık, Mw 7.8) using TEC data*, Acta Astronaut., 215, 234-244, doi: 10.1016/j.actaastro.2023.12.011.

Eroglu E.; 2023a: *Ionospheric anomalies probably related to the Mw 7.1 northern Mid-Atlantic Ridge earthquake*, Adv. Space Res., 71, 3382-3393, doi: 10.1016/j.asr.2022.12.010.

Eroglu E.; 2023b: *Ionospheric anomalies related to the Mw 6.5 Samar, Philippines earthquake*, Acta Geophys., 71, 601-611, doi: 10.1007/s11600-022-00980-8.

Eroglu E. and Başçiftçi F.; 2024: *Mathematical modeling of the southeastern Turkey earthquake (Pazarcık, Mw 7.8) using TEC data.* Acta Astronaut., 215, 234--244, doi: 10.1016/j.actaastro.2023.12.011.

Eroglu E., Nane E. and Göker U.D.; 2023: *Seismo-ionospheric anomalies related to the Mw 6.6, July 20, 2017, earthquake in Bodrum, Turkey*. Nat. Hazards, 117, 1521-1539, doi: 10.1007/s11069-023-05914-1.

Gonzalez W.D., Joselyn J.A., Kamide Y., Kroehl H.W., Rostoker G., Tsurutani B.T. and Vasyliunas V.M.; 1994: *What is a geomagnetic storm?.* J. Geophys. Res., 99, 5771. doi: 10.1029/93JA02867.

İnyurt S., Mekik Ç. and Yıldırım Ö.; 2020: *Deprem kaynaklı olabilecek* İyonosferik *değişimlerin belirlenmesi* üzerine *yeni bir yaklaşım geliştirilmesi*. Geomatik, 5, 127-133, doi: 10.29128/geomatik.592477.

Khan A.Q., Ghaffar B., Shah M., Ullah I., Oliveira-Júnior J.F. and Eldin S.M.; 2022: *Possible seismo-ionospheric anomalies associated with the 2016 Mw 6.5 Indonesia earthquake from GPS TEC and Swarm satellites*. Front. Astron. Space Sci., 9, doi: 10.3389/fspas.2022.1065453.

Lemmerer B. and Unger S.; 2019: *Modeling and pricing of space weather derivatives*. Risk Manage., 21, 265-291, doi: 10.1057/s41283-019-00052-0.

Leonard R.S. and Barnes R.A.; 1965: *Observation of ionospheric disturbances following the Alaska earthquake*. J. Geophys. Res., 70, 1250-1253, doi: 10.1029/JZ070i005p01250.

Liu J.Y., Chen Y.I., Chen C.H., Liu C.Y., Chen C.Y., Nishihashi M., Li J.Z., Xia Y.Q., Oyama K.I., Hattori K. and Lin C.H.; 2009: *Seismoionospheric GPS total electron content anomalies observed before the 12 May 2008 Mw7.9 Wenchuan earthquake*. J. Geophys. Res., 114, 04320, doi: 10.1029/2008JA013698 .

Liu Z. and Gao Y.; 2004: *Ionospheric TEC Predictions over a local area GPS reference network*. GPS Solutions, 8, 23-29, doi: 10.1007/s10291-004-0082-x.

Liu Z., Skone S., Gao Y. and Komjathy A.; 2005: *Ionospheric modeling using GPS data*. GPS Solutions, 9, 63-66, doi: 10.1007/s10291-004-0129-z.

Menvielle M. and Berthelier A.; 1991: *The K-derived planetary indices: description and availability*. Rev. Geophys., 29, 415-432, doi: 10.1029/91RG00994.

Morales A.M., Vazquez-Becerra G.E., Millan-Almaraz J.R., Pérez-Enríquez R., Martínez-Félix C.A. and Gaxiola-Camacho J.R.; 2020: *Examination of seismo-ionospheric anomalies before earthquakesof Mw ≥ 5.1 for the period 2008-2015 in Oaxaca, Mexico using GPS-TEC*. Acta Geophys., 68, 1229-1244, doi: 10.1007/s11600-020-00470-9.

Myagkova I.N., Shirokii V.R., Vladimirov R.D., Barinov O.G. and Dolenko S.A.; 2021: *Prediction of the Dst Geomagnetic index using adaptive methods*. Russ. Meteorol. Hydrol., 46, 157-162, doi: 10.3103/S1068373921030031.

Schaer S., Gurtner W. and Feltens J.; 1998: *IONEX: the ionosphere map exchange format version 1*. In: Proc. IGS, ESA/ESOC, Darmstadt, Germany, IGS, International GPS Service, pp. 233-248.

Schwenn R.; 2001: *Solar wind: global properties.* In: Paul Murdin (ed), Encyclopedia of Astronomy and Astrophysics, Institute of Physics Publishing, Bristol, UK, 2301, doi: 10.1888/0333750888/2301.

Shah M., Abbas A., Adil M.A., Ashraf U., Oliveira-Ju´nior J.F., Tariq M.A., Ahmed J., Ehsan M. and Ali A.; 2022: *Possible seismo-ionospheric anomalies associated with Mw > 5.0 earthquakes during 2000–2020 from GNSS TEC*. Adv. Space Res., 70, 179-187, doi: 10.1016/j.asr.2022.04.025.

Tang L., Li Z. and Zhou B.; 2018: *Large-area tsunami signatures in ionosphere observed by GPS TEC after the 2011 Tohoku earthquake*. GPS Solutions, 22, doi: 10.1007/s10291-018-0759-1.

Tariq M.A, Shah M., Hernàndez-Pajares M., Iqbal T.; 2019: *Pre-earthquake ionospheric anomalies before three majör earthquakes by GPS-TEC and GIM-TEC data during 2015-2017*, Adv. Space Res., 63, 2088-2099, doi: 10.1016/j.asr.2018.12.028.

Tariq M.A., Shah M., Li Z., Wang N., Shah M.A., Iqbal, T. and Liu. L.; 2021: *Lithosphere ionosphere coupling associated with three earthquakes in Pakistan from GPS and GIM TEC*, J. Geodyn. 147, 11 pp., 101860, doi: 10.1016/j.jog.2021.101860.

Ulukavak M.; 2016: *Ekvatoral ve Orta Kuşak Depremleri ile* İyonosferik *TEC Anomalileri Arasındaki* İlişkinin *Araştırılması (Investigation of the relationship between equatorial and mid-latitude earthquakes with ionospheric TEC anomalies)*. Karadeniz Teknik Üniversitesi, dissertation thesis, 112 pp., in English.

Ulukavak, M., Inyurt, S.; 2020: *Detection of possible ionospheric precursor caused by Papua New Guinea earthquake (Mw 7.5)*. Environ. Monit. Assess., 192 (190), 15 pp., doi: 10.1007/s10661-020-8146-0.

Zhu F., Zhou Y., Lin J. and Fu F.; 2014: *A statistical study on the temporal distribution of ionospheric TEC anomalies prior to M7.0+ earthquakes during 2003-2012*. Astrophys. Space Sci., 350, 449–457. doi: 10.1007/s10509-014-1777-2.

Corresponding author: Sercan Bülbül
Department of Geomatic Engineering, Faculty of Engineering and Natural Sciences, Konya Technical University
Ardıçlı, Rauf Orbay Cd., 42250 Selçuklu Konya, Turkey
Phone: +90 536 572 7639; e-mail: sbulbul@ktun.edu.tr